International Journal of Power Electronics and Drive System (IJPEDS)
Vol. 17, No. 4, December 2026, pp. 2335~2352
ISSN: 2088-8694, DOI: 10.11591/ijpeds.v17.i4.pp2335-2352

Comparative study of nonlinear state estimators for weighted recursive least squares assisted adaptive SOC estimation of sodium-ion batteries

Muhammad Firdaus Ishak[1], Mohd Junaidi Abdul Aziz[1], Mohd Ibthisham Ardani[2], Low Wen Yao[1], Tole Sutikno[3,4]

[1]Faculty of Electrical Engineering, Universiti Teknologi Malaysia, Johor, Malaysia
[2]Faculty of Mechanical Engineering, Universiti Teknologi Malaysia, Johor, Malaysia
[3]Department of Electrical Engineering, Faculty of Industrial Technology, Universitas Ahmad Dahlan, Yogyakarta, Indonesia
[4]Embedded System and Power Electronics Research Group, Yogyakarta, Indonesia

Article Info

Article history:

Received Jul 3, 2026
Revised Sep 6, 2026
Accepted Sep 13, 2026

Keywords:

Adaptive SOC estimation
Battery management system
First-order Thevenin model
Nonlinear state estimators
Sodium-ion battery
Weighted recursive least squares

ABSTRACT

Accurate state-of-charge (SOC) estimation in sodium-ion batteries (SIBs) under dynamic loading is challenging because of asymmetric charge/discharge polarization and time-varying equivalent circuit parameters. In this study, an online adaptive model based on a weighted recursive least-squares (WRLS) updated first-order Thevenin model is integrated with extended Kalman filter (EKF), unscented Kalman filter (UKF), and particle filter (PF) estimators. We tested the dynamic stress test (DST) and New European Driving Cycle (NEDC) profiles with the same model structure, OCV-SOC relationship, measured current-voltage data, and evaluation conditions. WRLS adaptation improved the SOC estimation errors for all estimators over fixed-parameter operation. The PF had the smallest DST SOC RMSE and MAE (0.6% and 0.5%, respectively), while the EKF had the smallest NEDC errors (0.7% and 0.6%, respectively). The EKF also gave the lowest terminal-voltage RMSE of 0.03233 V and 0.01511 V for DST and NEDC, respectively. The average execution time was 2.63 μs/sample, which is less than that of the UKF and PF. In general, the EKF is the most balanced option in terms of SOC accuracy, voltage tracking, computational efficiency, and practical implementation.

This is an open access article under the CC BY-SA license.

Corresponding Author:

Mohd Junaidi Abdul Aziz
Faculty of Electrical Engineering, Universiti Teknologi Malaysia
Skudai, Johor, 81300, Malaysia
Email: junaidi@utm.my

1. INTRODUCTION

Sodium-ion batteries (SIBs) have gathered growing interest as a potential energy storage technology because of their materials availability, cost potential, and suitability for large-scale energy storage and low- to medium-mobility applications [1]–[5]. State-of-charge (SOC) estimation is vital for safe, reliable, and efficient management of SIBs. SIBs can, however, be asymmetric, in which the polarization voltage changes in magnitude and relaxes with the direction of the current and operating condition. This can be due to direction-dependent sodium-ion transport, interfacial charge-transfer kinetics, and electrode relaxation processes. As a result, the same current level at the same SOC can result in varying transient voltage drops and recovery times when charging and discharging. Even if the charging and discharging OCV-SOC curves exhibit a small hysteresis, the occurrence of asymmetric polarization may be possible, as equilibrium OCV hysteresis and dynamic polarization are two different electrochemical phenomena [1], [6]–[8].

Model-based SOC estimation is a practical compromise between physical interpretation, estimation accuracy, and computational complexity. The first-order Thevenin model is widely used as it is the predominant battery dynamic that can be represented by an OCV source, an ohmic resistance, and a single resistance-capacitance polarization branch [8], [9]. However, it has parameters that are not fixed while it is working. The ohmic resistance and polarization characteristics may be different depending on the SOC, temperature, current excitation, and condition of the cell. Online parameter identification is thus a practical solution to tracking these changes without significantly increasing the model order. The measured current and terminal-voltage data are used to update the ohmic and polarization-related parameters with the aid of weighted recursive least squares (WRLS). The adaptation enables the model to track the variations of the effective polarization response, thus reducing the effects of non-uniform and time-varying battery behavior on voltage prediction and SOC estimation.

The SOC estimation performance also depends on the nonlinear state estimator used with the adaptive model. The extended Kalman filter (EKF) is appealing due to its moderate computational complexity, but the local linearization may lead to reduced accuracy in the case of strong nonlinearity. The unscented Kalman filter (UKF) does not require explicit linearization of the Jacobian and is based on propagating sigma points through the nonlinear model, while the particle filter (PF) is based on weighted particles to represent the state distribution and can handle non-Gaussian uncertainty [10]–[13]. While a few recent SIB studies have explored equivalent-circuit modelling [8], adaptive estimation [10] and fractional-order filtering [14]–[16] and learning-assisted approaches [17], a controlled and experimental comparison of the EKF, UKF, and PF with the same online-adapted model and the same validation data is still limited.

Hence, the present study proposes a WRLS-based first-order Thevenin model and compares the EKF, UKF, and PF under dynamic stress test (DST) and New European Driving Cycle (NEDC) profiles consistently. The major contributions are the online identification of ohmic and polarization-related parameters, a controlled comparison of three nonlinear estimators, a direct comparison with fixed-parameter implementations, and an evaluation of the accuracy–computation trade-off. The results show that the errors of SOC estimation are reduced by WRLS adaptation for all three estimators. EKF gives the best overall performance in terms of SOC accuracy, terminal-voltage tracking, computational efficiency, and implementation simplicity, while PF gives the highest DST SOC accuracy, thus making the EKF the preferred estimator for the conditions studied for practical application online.

2. METHOD

2.1. Experimental data and preprocessing

The main specifications of the sodium-ion battery used in this study are presented in Table 1. The tested cell is a HAKADI 186500 sodium-ion battery with a nominal capacity of 1.5 Ah and nominal voltage of 3.1 V. The cell has a mass of 37 $\pm$ 0.5 g, a diameter of 18.40 $\pm$ 0.1 mm, and a height of 65.30 $\pm$ 0.1 mm. Under the standard charging condition, the battery is charged at a continuous current of 0.75 A until the upper cut-off voltage of 4.1 V is reached. The standard discharge condition is 1.5 A continuous discharge, and the maximum continuous discharge current is less than 4.5 A, with a lower cut-off voltage of 1.5 V. The allowable discharge temperature is defined in the range from −30 to 60 ℃, which is the operating range used during the experimental tests and also serves as a reference for use in the calculation of SOC and in safe battery operation.

Table 1. Descriptions of the sodium-ion battery used

Parameter	Specification
Type	Sodium-ion battery
Model	HAKADI 186500 sodium-ion battery
Nominal capacity	1.5 Ah
Nominal voltage	3.1 V
Weight	37 $\pm$ 0.5 g
Dimension	Diameter: 18.40 $\pm$ 0.1 mm
	Height: 65.30 $\pm$ 0.1 mm
Standard charge	Continuous current: 0.75 A
	Cut-off voltage: 4.1 V
Standard discharge	Continuous current: 1.5 A
	Cut-off voltage: 1.5 V
Maximum continuous discharge current	<4.5 A
Temperature of discharge	-30-60 ℃

Figure 1 shows a block diagram of the experimental test setup for sodium-ion battery data acquisition. It is composed of a sodium-ion battery cell, a DC electronic load, a multi-range DC power supply, and computer-based battery test software. The required discharge current profiles are applied to the battery using the DC electronic load, and the charging process is carried out using the DC power supply according to the specified charging condition. The computer-based test software controls the test sequence and records the current and terminal voltage measured during the battery operation. The actual laboratory setup is depicted in Figure 2, consisting of the test software, battery cell connection, DC power supply, electronic load, and measurement instrument. With this arrangement, the current and terminal voltage response of the sodium-ion battery can be obtained for various operating profiles. The experimental data are recorded and then used to develop the equivalent circuit model, identify the parameters by the WRLS method, and estimate the SOC by the nonlinear state estimator analysis.

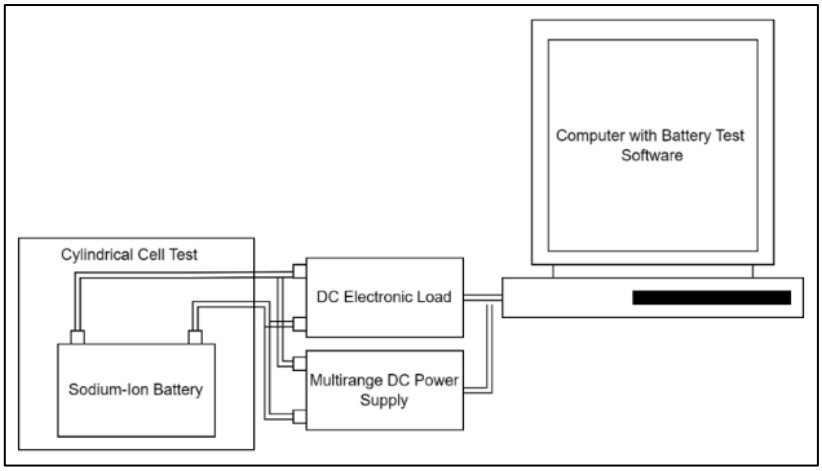

Figure 1. Block diagram of test setup

Figure 1 illustrates the experimental arrangement used to acquire the sodium-ion battery current and terminal-voltage data. The equipment included a sodium-ion battery cell, a programmable DC electronic load, a multi-range DC power supply, a measurement unit, and computer software for battery testing. The electronic load was used to apply the required discharge profiles, and the DC power supply was used to charge the system within specified current and voltage limits. The experimental sequence was controlled by the battery test software, and the current and terminal voltage were measured at 1st intervals. The experiments were performed with 5 sodium-ion cell(s) fresh cells that have less than 5 preliminary cycles. The cell was fully charged prior to each validation test and left to rest for 30 min to minimize transient polarization effects and to set a stable initial condition. The tests were performed at an ambient temperature of 27 °C, which was monitored using a Type-K thermocouple connected to a Pico Technology TC-08 thermocouple data logger. The current and terminal-voltage data recorded were checked, and no missing data or abnormal measurements were found. Hence, the entire data set was not filtered and was directly used for the identification of the WRLS parameters and the estimation of the SOCs. The experimental results thus obtained were then used to estimate the model parameters using WRLS and to assess the performance of the SOC estimation of the nonlinear state estimators. The laboratory setup is shown in Figure 2, consisting of the battery test fixture, DC power supply, electronic load, measurement instrument, and computer-based monitoring system.

Figure 3 presents the dynamic stress test (DST) profile used to evaluate the estimators under repeated and rapidly varying load conditions. The range of discharge pulses is from 0 A at rest to about 3.75 A at the highest load, with intermediate discharge levels of about 0.6, 0.9, 1.8 and 2.25 A. The total test time was approximately 9,300 s when the approximately 1,850-s current sequence was repeated until the battery's lower cut-off voltage was reached. The test was started from a fully charged state of the battery, and the measured battery terminal voltage was initially near 4.1 V, which is the upper cut-off limit, and was slowly reduced towards the lower cut-off limit of about 1.5 V as shown in Table 2. During the lower current and rest periods, there were polarization and voltage-recovery responses, which were slower than the ohmic voltage drops for each current transition. The DST profile was repeated several times, which makes it appropriate for testing the ability of WRLS to track the changes in the equivalent-circuit parameters and to compare the performance of the SOC estimation of the EKF, UKF and PF in the presence of strong dynamic loading [14]–[16].

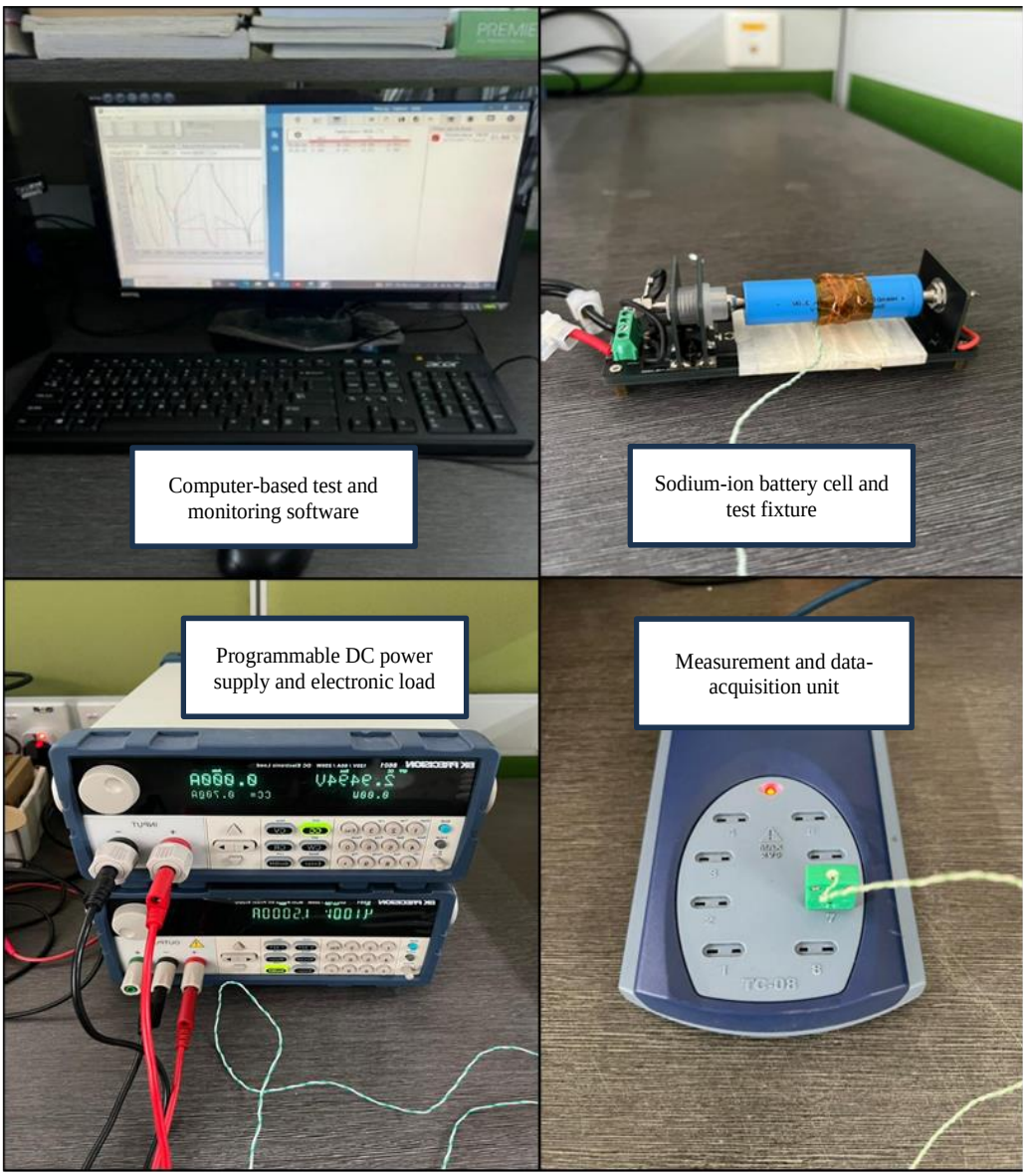

Figure 2. Laboratory setup for sodium-ion battery testing and data acquisition

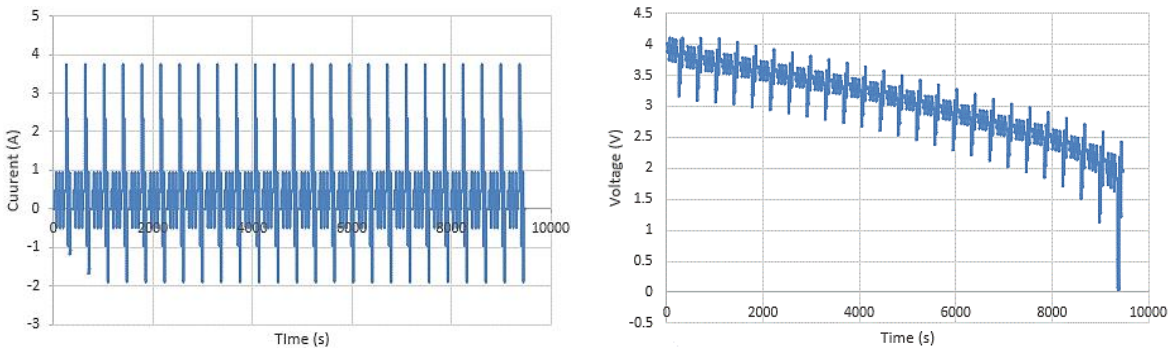

(a) (b)

Figure 3. DST test profile of the sodium-ion battery: (a) applied current profile and (b) applied voltage profile

Table 2. Experimental conditions for the evaluation profiles

Profile	Duration (s)	Current range (A)	Initial voltage (V)	Final voltage (V)
DST	9300	0-3.75	4.1	1.5
NEDC	1830	0-3.75	4.1	3.4

Figure 4 illustrates the NEDC profile employed as the second validation condition for assessing estimator performance under mobility-related loading. The test was performed for about 1850 s at an initial voltage of 4.1 as shown in Table 2, with a sampling interval of 1 s at 25 °C. The applied current was between 0 and around 3.75 A, with intermediate discharge currents of around 0.6, 0.9, 1.8, and 2.25 A. The profile did not include any negative current intervals, so no regenerative charging was included, and the zero current intervals were considered rest or zero-load conditions. During high current pulses, there were abrupt voltage drops caused by the ohmic and polarization effects, and voltage recovery during low current and rest intervals. Thus, the NEDC profile is used as another operating condition to test the performance of the EKF, UKF, and PF for time-varying current excitation to assess SOC and terminal-voltage estimation performance.

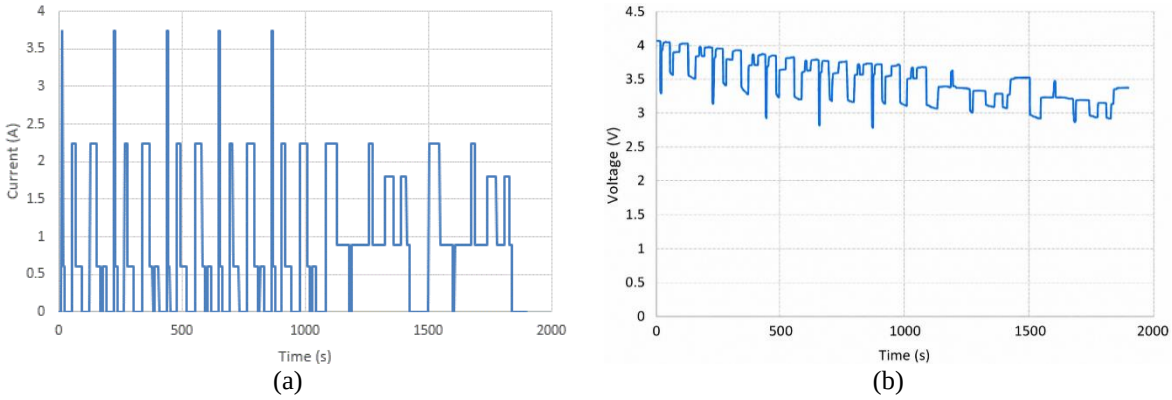

(a) (b)

Figure 4. NEDC test profile of the sodium-ion battery: (a) applied current profile and (b) applied voltage profile

2.2. Thevenin equivalent circuit model and OCV-SOC relation

The first-order Thevenin equivalent circuit model is used in this study to represent the electrical behavior of the sodium-ion battery with low model complexity. In this model, an open-circuit voltage source, an ohmic resistance, and a single RC polarization branch are used [10], [15], [18]–[21]. The model consists of an OCV source and an ohmic resistance R_0 and a single R_1C_1 polarization branch. The ohmic resistance corresponds to the voltage drop at the instant of application of the current, while the RC branch corresponds to the predominant transient polarization and relaxation response. The state vector includes the SOC and polarization voltage, which is represented as (1).

$$X(k) = \begin{bmatrix} SOC(k) \\ V_p(k) \end{bmatrix} \tag{1}$$

With positive current defined as discharge, the discrete SOC and polarization voltage equations are given by (2) and (3).

$$SOC\ (k+1) = SOC(k) - \frac{\eta I(k)\Delta t}{3600 Q_n} + \omega_{SOC}(k) \tag{2}$$

$$V_p = a(k)V_p(k) + b(k)I(k) + \omega_p(k) \tag{3}$$

Where:

$$a(k) = exp\left[-\frac{\Delta t}{R_1(k)C_1(\mathrm{k})}\right],\ b(k) = R_1(k)[1 - a(k)] \tag{4}$$

The terminal voltage is calculated from (5).

$$V_t(k) = OCV[SOC(k)] - R_0)(k)I(K) - V_p(k) + \upsilon(k) \quad (5)$$

Where Q_n is usable battery capacity, η is the coulombic efficiency, Δt is the sampling interval, and $\omega_{SOC}(k), \omega_p(k)$ and $\upsilon(k)$ represent process and measurement uncertainties. The OCV-SOC relationship was observed from experimental battery data and used the voltage reference in the measurement equation. The final manuscript should also include the details of the OCV extraction procedure, the rest condition, curve fitting method, goodness of fit value, and how the OCV derivative is calculated for the EKF.

The model parameters were not assumed constant over the operating profiles. WRLS algorithm, however, calculated online ohmic resistance and polarization-related coefficients based on the current and terminal voltage measured. The new parameters were then fed to EKF, UKF, and PF at the same sampling time to ensure that all the estimators are compared with the same adaptive battery model. The limitations were set on the parameters identified to keep the resistance and capacitance positive and the polarization coefficient $0 < a(k) < 1$.

Figure 5 shows the proposed adaptive SOC estimation framework based on the first-order Thevenin model. The current and voltage measured are first used to estimate the OCV and generate the voltage residual [15]. This residual is then fed into the online WRLS-based parameter identification block to update the Thevenin model parameters, particularly the ohmic resistance and the polarization-related coefficients [17]. New parameters are fed to the adaptive EKF for SOC estimation and error analysis of voltage. This structure enables the model to be responsive to parameter variations during battery operation while retaining a simple state-space representation. Thus, the first-order Thevenin model can be used for online SOC estimation as it offers a reasonable compromise between the accuracy of the model and the efficiency of computation and feasibility of real-time implementation.

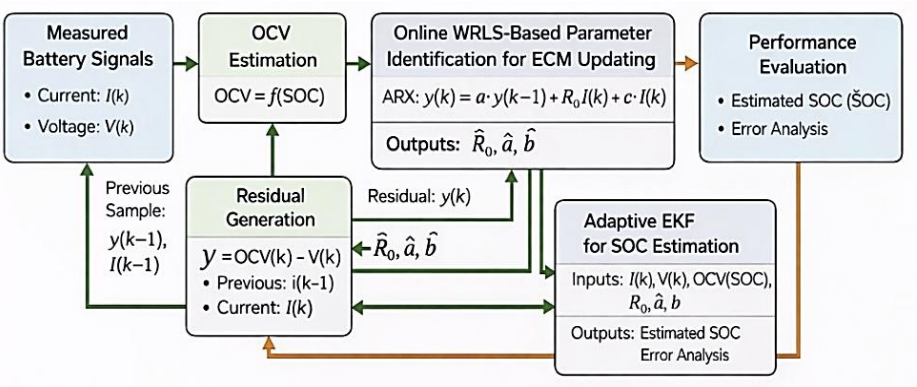

Figure 5. Proposed adaptive SOC estimation framework using online WRLS-based Thevenin parameter estimation model

2.3. WRLS online parameter identification

The parameters of the first-order Thevenin model were updated online using the weighted recursive least-squares (WRLS) algorithm. A first-order autoregressive model with an exogenous current input was used to represent the voltage behavior. The voltage residual $y(k)$ was defined similarly to the one implemented in the Simulink model, and the regressor vector comprised the previous voltage residual and the current and previous current samples. The identified model is written as (6).

$$y(k) = a(k)y(k-1) + R_0(k)I(k) + c(k)I(k-1) + \varepsilon(k) \quad (6)$$

Where $\varepsilon(k)$ defines the identification error. The parameter and regressor vectors are written as (7).

$$\theta(k) = [a(k) \quad R_0(k) \quad c(k)]^T, \phi(k) = [y(k-1) \quad I(k) \quad I(k-1)^T] \quad (7)$$

At each sampling instant, the prediction error is calculated as (8):

$$e(k) = y(k) - \phi^T(k)\theta(k-1) \quad (8)$$

and the recursive gain is obtained from:

$$K(k) = \frac{P(k-1)\phi(k)}{\lambda+\phi^T(k)P(k-1)\phi(k)} \quad (9)$$

Where λ is the forgetting factor and $P(k)$ is the covariance matrix. The parameter vector and covariance matrix are subsequently updated according to (10) and (11).

$$\theta(k) = \theta(k-1) + K(k)e(k) \quad (10)$$

$$P(k) = \lambda^{-1}[P(k-1) - K(k)\phi^T(k)P(k-1)] \quad (11)$$

The forgetting factor gives greater weight to recent measurements, allowing the model to respond to gradual changes in the battery parameters caused by SOC variation and dynamic current excitation.

The online WRLS parameter identification method is used to update the first-order Thevenin model parameters during battery operation. The behavior of the battery voltage is represented by an ARX model as indicated in Table 3, where the current state of the battery voltage is related to the past state of the battery voltage and the current and past current samples [22], [23]. The parameter vector $\theta = [a, R_0, c]^T$ is estimated recursively by means of the voltage residual error $e(k)$, recursive gain $K(k)$ and covariance matrix, P. The forgetting factor λ is used to give more weight to the data that has been gathered more recently, enabling the model to adjust if the battery parameters are altered by changing SOC, dynamic current loading, or polarization effects. The identified ARX parameters are then transformed into equivalent circuit model parameters. R_0 and the recovered polarization-related parameter $b = c + aR_0$ after the WRLS update. This online updating process makes the SOC estimation framework more robust, as the estimator will use updated model parameters rather than fixed offline parameters. Hence, the WRLS method enhances the adaptability of the first-order Thevenin model, and it can help to reduce the mismatch in voltage prediction in the case of rapid current variation. The proposed framework is thus simple to implement for real-time use and can track the major parameter variations of the sodium-ion battery in dynamic operation.

Table 3. Adaptive WRLS-1RC SOC estimation model

Model	Value
ARX model and parameter vector	$V(k) = ay(k-1) + R_0 I(k) + cI(k-1)$ $\theta = [a, R_0, c]^T$
Kalman Gain and estimation error	$K(k) = \frac{P\emptyset}{\lambda + \emptyset^T + P\emptyset}$ $e(k) = y(k) - \emptyset^T\theta$
Parameter and covariance update	$\theta = \theta + K(k)e(k)$ $P = \frac{1}{\lambda}(P - K\emptyset^T P)$
Recovered ECM parameter	$b = c + aR_0$

2.4. Nonlinear state estimators and benchmarking metrics

2.4.1. Nonlinear state estimators for SOC estimation

The same nonlinear battery model, measured current and terminal voltage, OCV-SOC relationship, and WRLS-updated equivalent circuit parameters were used to implement the EKF, UKF, and PF. This common implementation ensures that differences in estimation performance are mainly associated with the state-estimation method rather than differences in the underlying battery model. The nonlinear state and measurement equations are given by (12) and (13).

$$X_k = f(X_{k-1}, u_{k-1}) + w_{k-1} \quad (12)$$

$$z_k = h(X_k, u_k) + V_k \quad (13)$$

Where $X(k) = [SOC_k \quad V_{p,k}]^T$ is the state vector, U_k contains the measured current and z_k is the measured terminal voltage. The terms w_{k-1} and v_k represent the process and measurement noise, respectively.

The extended Kalman filter (EKF) is employed as the baseline nonlinear state estimator for SOC estimation using the same first-order Thevenin battery model [9], [12], [24], [25]. EKF estimates the battery states by linearizing the nonlinear state and measurement functions around the current operating point. During the prediction stage, the state estimate and error covariance are propagated from the previous corrected state as (14) and (15).

$$\hat{X}_{k|k-1} = f(\hat{X}_{k-1|k-1}, u_{k-1}) \tag{14}$$

$$\mathrm{P}_{k|k-1} = \mathrm{F}_k \mathrm{P}_{k-1|k-1} \mathrm{F}_k^T + \mathrm{Q}_k \tag{15}$$

Where F_k is the Jacobian of the state-transition function and Q_k is the process-noise covariance matrix. The predicted terminal voltage is evaluated from the predicted state as (16).

$$\hat{z}_k = h(\hat{X}_{k|k-1}, u_k) \tag{16}$$

The Kalman gain is then calculated using (17).

$$\mathrm{K}_k = \mathrm{P}_{k|k-1} \mathrm{H}_k^T \left(\mathrm{H}_k \mathrm{P}_{k|-1} \mathrm{H}_k^T + \mathrm{R}_k\right)^{-1} \tag{17}$$

Where H_k is the Jacobian of the measurement function and R is the measurement-noise covariance. The corrected state is then obtained from (18).

$$\hat{X}_{k|k} = \hat{X}_{k|k-1} + \mathrm{K}_k(\mathrm{Z}_k - h(\hat{X}_{k|k-1}, u_k)) \tag{18}$$

Therefore, the measurement at the current sampling time k is compared with the terminal voltage that is predicted from the previous state at $k-1$ directly, but with $\hat{X}_{k|k-1}$. When the battery model has a higher degree of nonlinearity, the EKF may suffer from local linearization, but it has a relatively simple recursive structure and low computational load.

The unscented Kalman filter (UKF) is applied to enhance the nonlinear state estimation without explicit linearization of the battery model [11], [12], [24]. The UKF does not explicitly use Jacobian linearization; instead, the state distribution is represented by a set of $2n+1$ sigma points, where n is the dimension of the state vector. The sigma points are created around the previous state estimate based on (19) and (20).

$$X_{k-1}^{(0)} = \hat{X}_{k-1|k-1} \tag{19}$$

$$X_{k-1}^{(i)} = \hat{X}_{k-1|k-1} \pm \sqrt{(n+\lambda)\mathrm{P}_{k-1|k-1}} \tag{20}$$

Where:

$$\lambda = a^2(n+k) - n \tag{21}$$

and α, β and κ are the UKF scaling parameters. Each sigma point is propagated through the nonlinear state function,

$$X_k^{(i)} = f(X_{k-1}^{(i)}, u_{k-1}) \tag{22}$$

and the predicted state is calculated from the weighted mean,

$$\hat{X}_{k|k-1} = \sum_{i=0}^{2n} W_i^{(m)} X_{k|k-1}^{(i)} \tag{23}$$

the predicted covariance is obtained by (24).

$$\mathrm{P}_{k|k-1} = \sum_{i=0}^{2n} W_i^{(c)} \left(X_{k|k-1}^{(i)} - \hat{X}_{k|k-1}\right)^2 + \mathrm{Q}_k \tag{24}$$

For the measurement update, the propagated sigma points are transformed through the nonlinear voltage equation:

$$\zeta_k^{(i)} = h(X_k^{(i)}, u_k) \tag{25}$$

and the predicted terminal voltage is (26).

$$\hat{z}_k = \sum_{i=0}^{2n} W_i^{(m)} \zeta_k^{(i)} \tag{26}$$

The measurement covariance and state-measurement cross-covariance are then calculated as (27) and (28).

$$\mathrm{S}_k = \sum_{i=0}^{2n} W_i^{(c)} \left(\zeta_k^{(i)} - \hat{z}_k\right)\left(\zeta_k^{(i)} - \hat{z}_k\right)^T + \mathrm{R} \tag{27}$$

$$\mathrm{C}_{xz,k} = \sum_{i=0}^{2n} W_i^{(c)} \left(X_k^{(i)} - \hat{x}_{k|k-1}\right)\left(\zeta_k^{(i)} - \hat{z}_k\right)^T \tag{28}$$

The UKF and corrected state estimates are subsequently given by (29) and (30).

$$\mathrm{K}_k = \mathrm{C}_k \mathrm{S}_k^{-1} \tag{29}$$

$$\hat{X}_{k|k} = \hat{X}_{k|k-1} + \mathrm{K}_k(\mathrm{Z}_k - \hat{\mathrm{Z}}_k) \tag{30}$$

UKF does not require explicit derivatives, unlike EKF, and it propagates the nonlinear state distribution, which may be beneficial in nonlinear state estimation of OCV-SOC and terminal-voltage response. However, the generation and propagation of sigma points results in a higher computational load compared to EKF.

The PF estimates the battery states assuming a set of Np weighted particles, instead of a Gaussian distribution of states [11]. Each particle is propagated in the nonlinear state model as (31).

$$X_k^{(i)} = f\left(X_{k-1}^{(i)}, u_{k-1}\right) + w_{k-1}^{(i)}, i = 1, \ldots, N_p \tag{31}$$

Where $w_{k-1}^{(i)}$ defines the process noise applied to the i-th particle. The predicted terminal voltage of each particle is obtained from (32).

$$\hat{z}_k = h(X_k^{(i)}, u_k) \tag{32}$$

The particle weight is updated according to the likelihood of the measured voltage:

$$\widetilde{w}_k = w_{k-1}^{(i)} p(z_k | X_k^{(i)}) \tag{33}$$

where, assuming Gaussian measurement noise.

$$p(z_k | X_k^{(i)}) \propto exp\left[-\frac{1}{2}\left(z_k - \hat{z}_k^{(i)}\right)^T \mathrm{R}^{-1}\left(\left(z_k - \hat{z}_k^{(i)}\right)\right]\right. \tag{34}$$

The weights are normalized as (35):

$$w_k^{(i)} = \frac{w_k^{(i)}}{\sum_{j=1}^{Np} w_k^{(i)}} \tag{35}$$

and the estimated state is obtained from the weighted particle mean,

$$\hat{X}_k = \sum_{i=1}^{Np} w_k^{(i)} X_k^{(i)} \tag{36}$$

Particle degeneracy is monitored using the effective number of particles,

$$N_{eff} = \frac{1}{\sum_{i=1}^{Np}\left(w_k^{(i)}\right)^2} \tag{37}$$

and resampling is performed when N_{eff} falls below the specified threshold. The PF can represent nonlinear and non-Gaussian state uncertainty more flexibly, but its computational requirement is high compared to EKF and UKF.

2.4.2. Estimator tuning parameters and metrics

The estimation performance is assessed using root mean square error (RMSE) and mean absolute error (MAE) as shown in (38) and (39). RMSE is a measure of the overall variance between the reference value, x_i and the estimated value, $\hat{x}_i$ with higher mistakes given greater weight due to the squared term [11],

[26]. Therefore, the RMSE is useful for identifying large errors in the estimation of dynamic current changes. Meanwhile, MAE is calculated as the average absolute difference between the reference value and the estimated value, which directly shows the overall accuracy of the estimation [9], [11], [26]. The performance of the EKF, UKF, and PF algorithms in terms of both metrics is evaluated in this work for different test profiles.

$$RMSE = \sqrt{\frac{1}{N}}\sum_{i=1}^{N}(\hat{x}_i - x_i)^2 \quad (38)$$

$$MAE = \frac{1}{N}\sum_{i=1}^{N}(\hat{x}_i - x_i) \quad (39)$$

3. RESULTS AND DISCUSSION

3.1. OCV-SOC fitting and WRLS parameter tracking

Figure 6 presents the OCV–SOC fitting result obtained from the sodium-ion battery test data. The fitted curve is monotonic, and the OCV increases with increasing SOC, ranging from around 2.0 V at low SOC to around 4.1 V at full SOC. This trend shows that the relationship between the OCV and SOC of the sodium-ion cell is not linear, but the selected fitting function can well represent the trend of the sodium-ion cell. The fitting errors, shown in the residual plot, are mostly concentrated around zero, and the majority of the errors are within a few millivolts. This means that the fitted OCV curve is appropriate to be used as the voltage reference for the SOC estimation model. But there are some residual peaks remaining at some SOC points, particularly in the low-to-middle SOC region. These deviations can be attributed to relaxation effects, measurement noise, and asymmetric polarization behavior of sodium-ion batteries under charge and discharge.

Figure 7 shows the online estimation of the ohmic resistance, R_0, using the WRLS algorithm. The value of R_0 is not constant throughout the test and changes with the operating condition of the battery. Initially, R_0 is about 0.24–0.25 Ω, and then gradually rises to a maximum value of about 0.29 Ω in the midsection of the profile. Following this, the resistance gradually drops off towards the end of the test. This variation demonstrates the influence of dynamic current excitation, SOC operating region, and electrochemical polarization on the internal resistance of the sodium-ion battery. Thus, the fixed resistance value may not be very accurate in the Thevenin model, particularly under dynamic load profiles. The WRLS update also enables R_0 to be adjusted online, enhancing the model's ability to track the actual battery voltage response.

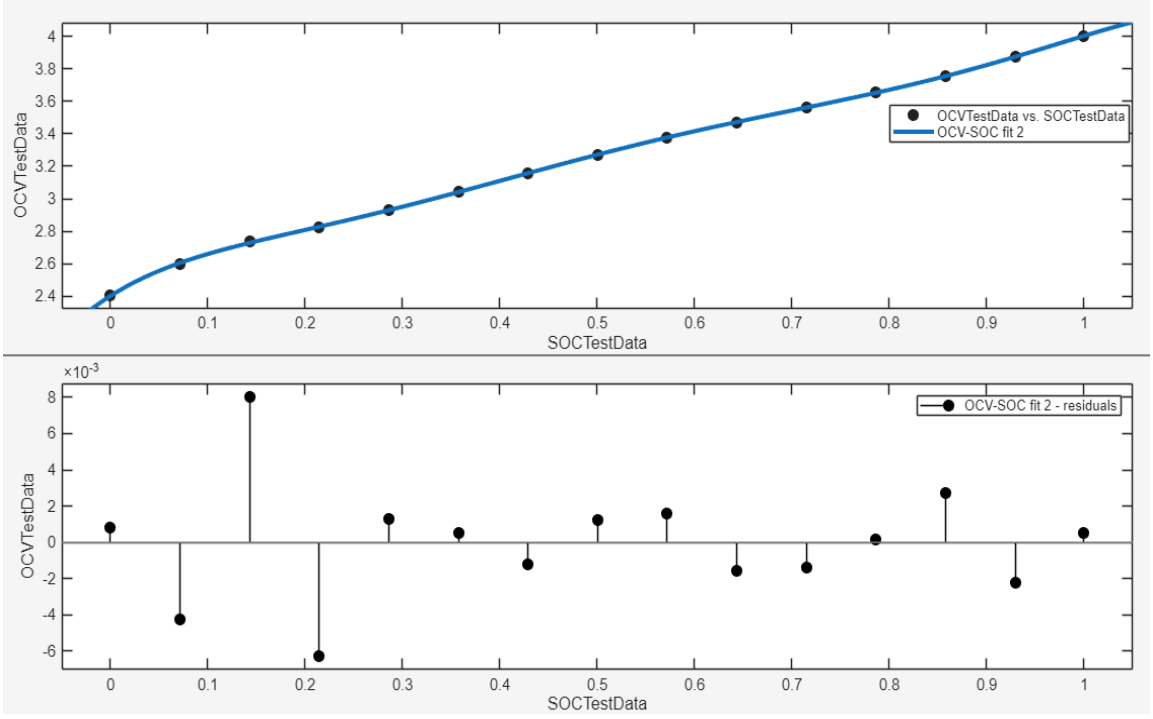

Figure 6. OCV-SOC fitting using MATLAB with residual values

Figure 8 depicts the estimated polarization parameters a and b, which define the transient voltage behavior of the first-order Thevenin model. The parameters a climb from 0.05 to nearly 0.1 before gradually decreasing, while b changes from roughly -0.03 to -0.015 and then decreases again at the end of the test. These variations show that the battery polarization dynamics vary over time and are influenced by the applied current profile. The smooth variations in both parameters demonstrate that WRLS can follow the parameter variation while avoiding unstable oscillations. Overall, Figures 7 and 8 depict that the WRLS technique is appropriate for adaptive parameter identification in sodium-ion battery modelling, where ohmic and polarization characteristics cannot be presumed constant during operation.

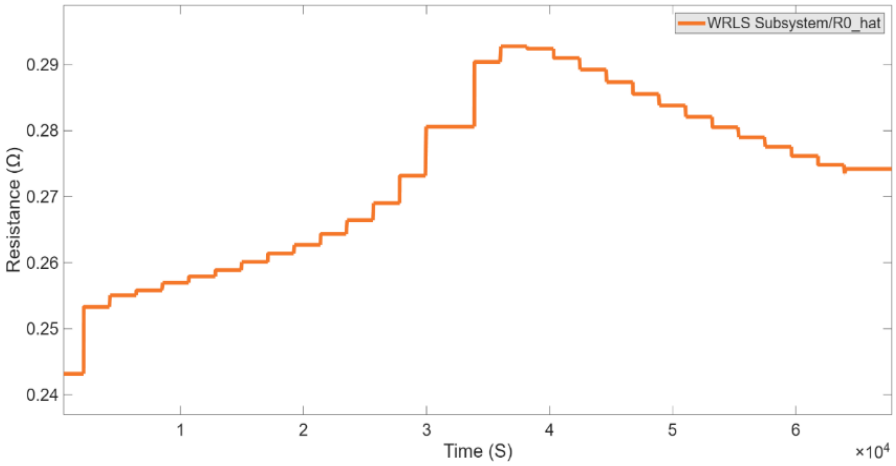

Figure 7. Ohmic R_0 parameter difference estimated by WRLS algorithm

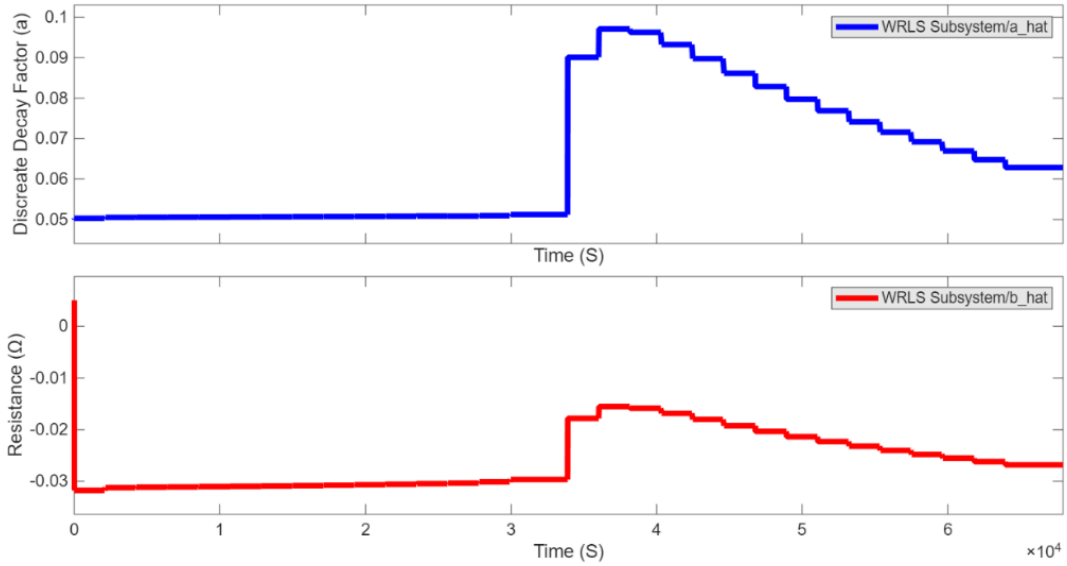

Figure 8. Polarization parameters a and b estimated by the WRLS algorithm

3.2. SOC estimation under DST and NEDC profiles

The performance of the EKF, UKF, and PF has been assessed by comparing their estimated SOC values to the Coulomb-counting (CC) reference for the DST and NEDC operating profiles, respectively, as illustrated in Figures 9 and 10. In the highly dynamic DST profile, none of the three estimators showed significant deviations from the overall decreasing trend of the reference SOC. The differences in the estimators were more noticeable during the rapid current variations and in the low-SOC region, where the voltage-estimation error may affect the state-correction process. As shown in Table 4, the PF had the highest accuracy with an RMSE of 0.6% and an MAE of 0.5%. EKF achieved an RMSE of 1.7% and an MAE of

1.1%, whereas UKF had the highest error with an RMSE of 2.7% and an MAE of 2.3%. The results show that the PF is more stable under rapidly changing load conditions, as it is able to represent the particles in a way that allows for a more effective representation of nonlinear behavior and estimation uncertainty.

All three estimators showed better and more stable tracking of the SOC under the NEDC profile than under the DST profile as in Table 4. EKF had the smallest errors, with RMSE of 0.7% and MAE of 0.6%, which were very close to PF with RMSE and MAE of 0.8%. The UKF had relatively large errors with an RMSE of 1.9% and an MAE of 1.4%. The lower errors achieved in the NEDC indicate that the relatively smooth current variation in the NEDC results in lower transient voltage errors and more stable SOC correction of the WRLS-updated Thevenin model parameters. Thus, the EKF performs best in the NEDC profile, while the PF performs better in the more dynamic DST profile. This comparison verifies that the accuracy of the estimator depends on the current-excitation properties and the dynamics of the batteries.

Finally, the SOC estimation results demonstrate that the WRLS-assisted adaptive Thevenin framework is able to help in stable SOC tracking under both DST and NEDC operating profiles. But the optimal nonlinear estimator is a function of the battery operating condition. Under the condition of a smoother dynamic profile, the EKF is more suitable for the estimation of SOC due to its simple implementation and more accurate estimation results, and the PF is more suitable for the case of high dynamic load excitation because its uncertainty representation is stronger. The results demonstrate that the selection of the estimator for sodium-ion battery BMS should consider the characteristics of the current profile, as well as the dynamic operating condition of the battery.

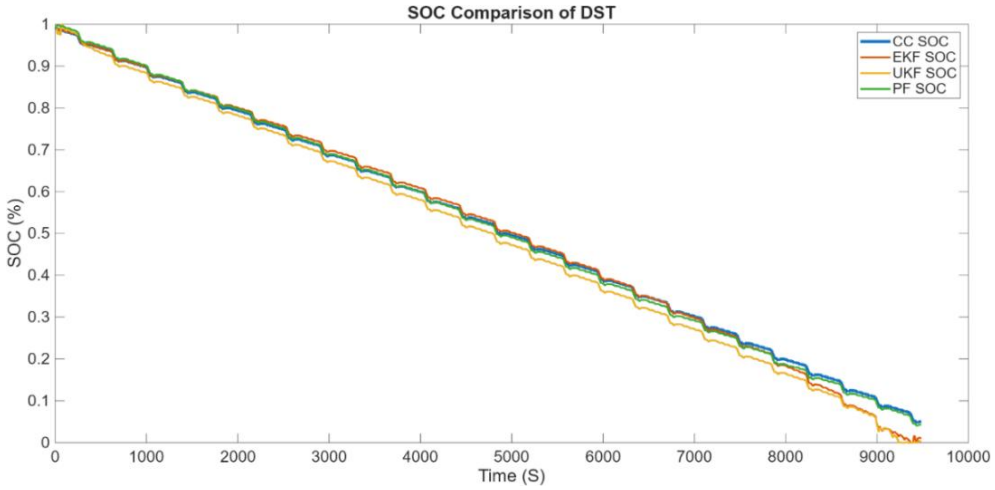

Figure 9. SOC comparison of DST cycle

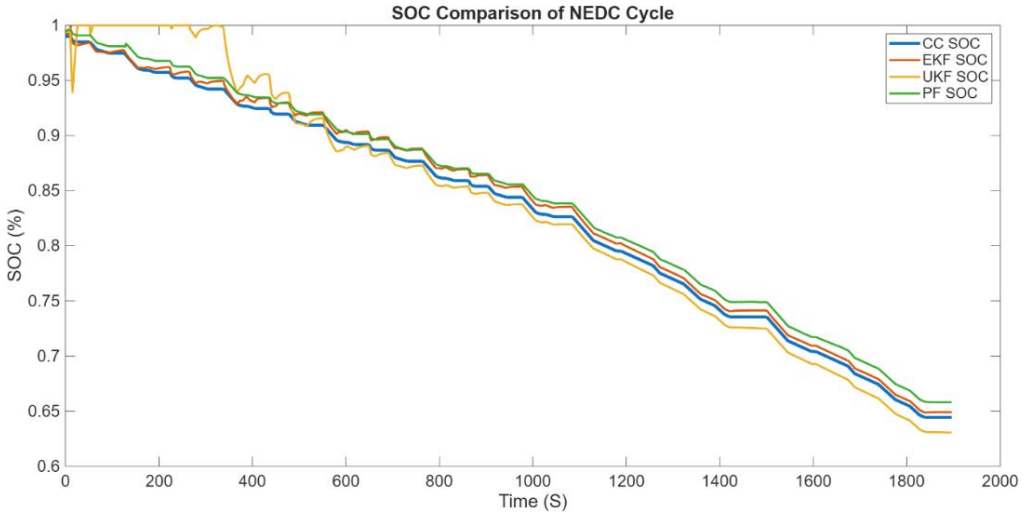

Figure 10. SOC comparison of NEDC cycle

Table 4. Error analysis of SOC using RMSE and MAE

Algorithms	Battery test cycle	Error analysis	Results analysis (%)	Algorithms	Battery test cycle	Error analysis	Results analysis (%)
EKF	DST	RMSE	1.7	PF	DST	RMSE	0.6
		MAE	1.1			MAE	0.5
	NEDC	RMSE	0.7		NEDC	RMSE	0.8
		MAE	0.6			MAE	0.8
UKF	DST	RMSE	2.7				
		MAE	2.3				
	NEDC	RMSE	1.9				
		MAE	1.4				

3.3. Terminal voltage tracking and comparative performance

Figures 11 and 12 compare the measured terminal voltage with the voltages reconstructed using the EKF, UKF, and PF under the DST and NEDC profiles, respectively. The RMSE is used as the main performance measure, since it places a higher weight on voltage deviations that occur during fast load switching, while the MAE measures the average value of the voltage estimation error. These indicators can be used together to have a more complete picture of the overall accuracy of the voltage tracking and how sensitive each estimator is to the transient errors.

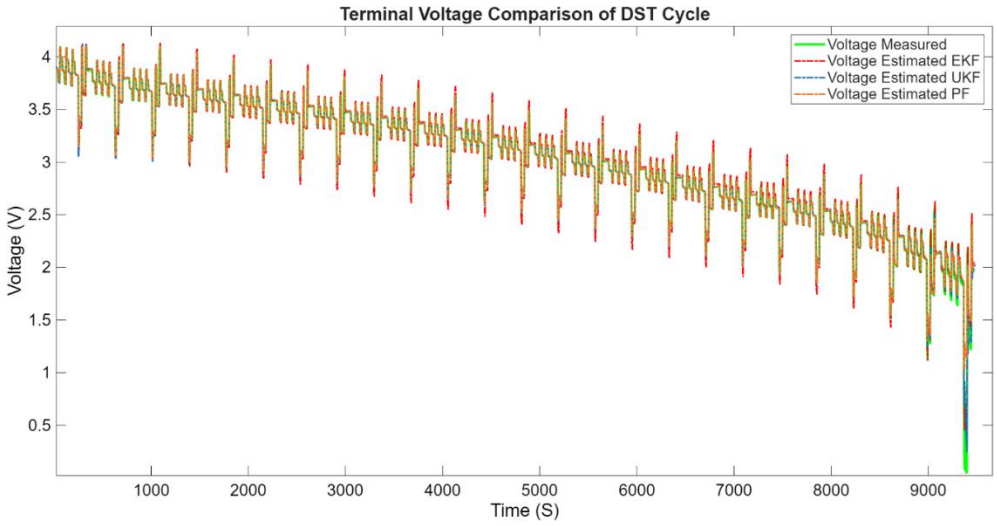

Figure 11. Terminal voltage estimation performance under DST cycle

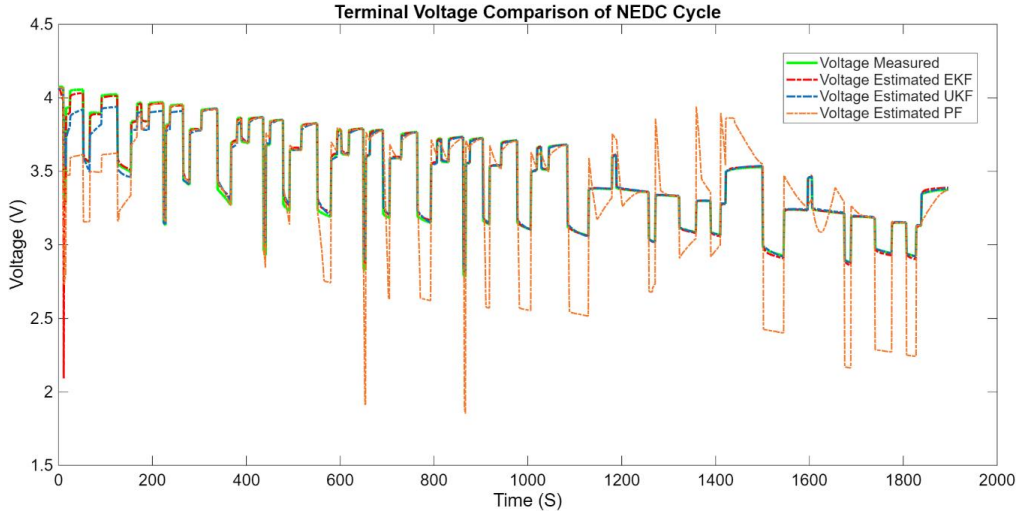

Figure 12. Terminal voltage estimation performance under NEDC cycle

The DST profile generates significant terminal-voltage fluctuations from the high-frequency current changes, which result in ohmic voltage drops and polarization effects. All three estimators track the overall trend of the measured voltage, but there are differences seen during abrupt voltage drops and recovery. As shown in Table 5, the EKF has the lowest RMSE and MAE of 0.03233 V and 0.012209 V, respectively. The performance of the UKF is similar, with an RMSE of 0.03900 V and an MAE of 0.01232 V. The PF gives the highest RMSE of 0.06022 V, but its MAE of 0.01384 V is still pretty close to those of the EKF and UKF. The higher value of the PF RMSE compared to its MAE suggests that there were a few relatively large voltage deviations in the transient period. However, the low SOC error obtained by the PF despite DST shows that the best tracking accuracy of the SOC does not necessarily translate into the lowest reconstruction error of the terminal voltage. Thus, the accuracy of the SOC estimation and the agreement of the terminal voltage should be assessed independently.

With the NEDC profile, the EKF reconstruction of the terminal voltage is the most accurate, with RMSE of 0.01511 V and MAE of 0.005044 V. These values are significantly reduced compared to the DST values and are a sign of better voltage tracking under the NEDC operating condition. The results from UKF have an RMSE of 0.03945 V and an MAE of 0.01828 V, which are greater than those achieved by EKF. Although the performance under the DST profile is similar to that of the other profiles, the relatively high PF values for both error indicators indicate that the voltage-tracking deviations are not confined to a few isolated transients and is a more consistent behavior throughout the NEDC cycle. These results can be related to the PF likelihood calculation, particle distribution, resampling process, or the chosen process- and measurement-noise parameters.

In general, the RMSE and MAE results show that EKF gives the best tracking of the terminal voltage in both operating profiles. The UKF results are very similar to the EKF result under DST, but do not match the EKF under NEDC. The terminal-voltage reconstruction of the PF shows lower accuracy, especially under NEDC, while the accuracy of the SOC estimation is the highest under DST. The results show that the more complex the estimator, the better the voltage reconstruction is not always true when the same equivalent-circuit model and WRLS-updated parameters are used for all the estimators. Hence, the selection of the estimator practically should consider the accuracy of SOC, the terminal-voltage error, the convergence behavior, the complexity of implementation, and the computational time. The WRLS-assisted EKF is found to be the most balanced method for online SOC and terminal-voltage estimation for sodium-ion batteries operating under dynamic conditions, due to its consistently low voltage errors and good SOC estimation accuracy.

Table 5. Statistical error of terminal voltage estimation

Algorithms	Battery test cycle	Error analysis	Results analysis (V)
EKF	DST	RMSE	0.03233
		MAE	0.012209
	NEDC	RMSE	0.01511
		MAE	0.005044
UKF	DST	RMSE	0.039
		MAE	0.01232
	NEDC	RMSE	0.03945
		MAE	0.01828
PF	DST	RMSE	0.06022
		MAE	0.01384
	NEDC	RMSE	0.135
		MAE	0.08221

3.4. Contribution of WRLS parameter adaptation

Table 6 shows the performance of the fixed-parameter and WRLS-assisted estimators for the DST and NEDC profiles. All three estimators have better SOC accuracy with the WRLS adaptation. The improvements are 73.0% and 75.0% for the EKF, respectively, under DST and NEDC, and the SOC RMSE is reduced from 6.3% to 1.7% under DST and from 2.8% to 0.7% under NEDC. The UKF reduces the RMSE by 54.2% under DST and 42.4% under NEDC. WRLS adaptation also improves the performance of the PF, especially under DST, with the RMSE and MAE reducing from 1.8% and 1.7% to 0.6% and 0.5%, respectively. Under NEDC, the corresponding PF errors decrease from 1.0% to 0.8%. These results demonstrate that online parameter adaptation is effective for enhancing the SOC estimation in the case of dynamic operation, where the battery parameters vary.

The adaptation of WRLS has different effects on voltage estimation, depending on the estimator used. For the UKF, the voltage RMSE decreases from 0.1138 to 0.03900 V under DST and from 0.1241 to 0.03945 V under NEDC. Similarly, the PF voltage RMSE decreases from 0.1726 to 0.06022 V under DST

and from 0.1587 to 0.135 V under NEDC. In contrast, the EKF voltage RMSE increases slightly from 0.02268 to 0.03233 V under DST and from 0.01140 to 0.01511 V under NEDC. This increase is because the parameters used in the WRLS are different depending on the current excitation, and the voltage reconstructed by the WRLS will slightly change due to the small transient changes. The adaptive parameters enhance the internal state representation and SOC correction but not necessarily reduce the voltage residual at each sampling time. However, the RMSE of the voltage estimate produced by the WRLS-assisted EKF is the lowest for both profiles compared to the two other adaptive estimators. In conclusion, WRLS adaptation consistently improves SOC estimation, with the PF providing the highest SOC accuracy and the EKF offering the best overall balance between SOC and terminal-voltage accuracy.

Table 6. Fixed-parameter and WRLS-assisted estimator comparison

Estimator	Profile	Parameter mode	SOC RMSE (%)	SOC MAE (%)	Voltage RMSE (V)
EKF	DST	Fixed	6.3	5.8	0.02268
		WRLS	1.7	1.1	0.03233
	NEDC	Fixed	2.8	2.7	0.01140
		WRLS	0.7	0.6	0.01511
UKF	DST	Fixed	5.9	3.9	0.1138
		WRLS	2.7	2.3	0.039
	NEDC	Fixed	3.3	1.6	0.1241
		WRLS	1.9	1.4	0.03945
PF	DST	Fixed	2.8	2.7	0.1726
		WRLS	0.6	0.5	0.06022
	NEDC	Fixed	1.0	1.0	0.1587
		WRLS	0.8	0.8	0.135

3.5. Computational burden and real-time feasibility

The computational demands of the EKF, UKF, and PF are summarized in Table 7 for the same number of estimator calls (9490) under the same simulation conditions. The EKF has the least computational load, with a total execution time of 0.025 s and an average execution time of 2.63 μs per sample. The total time the UKF takes is 0.249 s and 26.24 μs per sample, while the PF takes the longest time of 1.277 s and 134.56 μs per sample, respectively. This implies that the computational demands of the UKF and PF are around 10 and 51 times greater than the EKF.

The generation and propagation of sigma points are the cause of the higher computational cost of the UKF. The PF needs extra computation to facilitate propagation of particles, evaluation of likelihood, normalization of weights, and resampling. However, the average execution times of all three estimators are still less than 1 ms per sample, indicating that they may be suitable to be implemented in real-time if the sampling interval is greater than the required computation. The results reported, however, are for the estimator execution only, and do not include other operations used for WRLS parameter identification, data acquisition or hardware communication. In conclusion, the EKF provides the highest computational efficiency, whereas the improved SOC accuracy of the PF under highly dynamic conditions is achieved at the expense of substantially greater computational burden.

Table 7. Computational requirements of the nonlinear estimators

Estimator	Number of calls	Total core execution time (s)	Average time/sample (μs/sample)
EKF	9490	0.025	2.63
UKF	9490	0.249	26.24
PF	9490	1.277	134.56

3.6. Practical discussion on adaptive estimation framework

The first-order Thevenin model is a practical compromise between model accuracy and computational complexity and is suitable for online SOC estimation. Its ohmic resistance is the voltage drop at an instant; the ohmic response is captured by a single RC branch during battery operation. However, it is not possible to fully describe the parameter variations that may occur with changes in the SOC and dynamic current excitation with fixed model parameters. To overcome this drawback, the WRLS algorithm is proposed to update the model parameters in an online manner, thus enhancing the model representation of the asymmetric polarization behavior of the sodium-ion battery. The results in comparison with the fixed-parameter approach indicate that the adaptation of WRLS decreases the SOC RMSE for all three estimators for both DST and NEDC profiles. However, it has been found to be estimator-dependent, which means that better state estimation does not necessarily result in the smallest voltage residual at each sampling time.

Results from the estimator show that there is a trade-off between SOC accuracy, voltage tracking, and computational complexity. The PF has the highest accuracy of SOC under DST with an RMSE of 0.6% and an MAE of 0.5%, while the EKF has the lowest SOC errors under NEDC with an RMSE of 0.7% and an MAE of 0.6%. The EKF also yields the smallest voltage RMSE for both operating profiles, and it consumes 2.63 μs per sample, while the UKF and the PF consume 26.24 μs and 134.56 μs per sample, respectively. Hence, the PF is beneficial if the most important requirement is SOC accuracy under strong dynamic excitation, while the EKF can offer the most balanced performance for practical implementation. In conclusion, the WRLS-assisted EKF is suitable for real-time sodium-ion battery management systems due to its high estimation accuracy, low computational complexity, and ability to track voltage.

4. CONCLUSION

In conclusion, the proposed adaptive framework provides a practical approach for SOC estimation in sodium-ion batteries by integrating a first-order Thevenin model, WRLS-based online parameter identification, and nonlinear state estimators. The WRLS adaptation method is able to increase the accuracy of the SOC, which is not possible with the fixed-parameter method due to the variations in the parameters under dynamic operating conditions. PF provides the best SOC accuracy in the highly dynamic DST profile, while the EKF gives the lowest SOC error under NEDC. Moreover, EKF has the lowest terminal-voltage RMSE for both profiles and the lowest average computation time of 2.63 μs per sample. The PF is more capable of uncertainty representation but requires about 51 times more computation than the EKF. Thus, the WRLS-assisted EKF is the most balanced estimator in terms of the accuracy of the SOC estimation, voltage tracking, computational complexity, and implementation complexity, and is the most suitable estimator for a real-time sodium-ion battery management system.

FUNDING INFORMATION

The authors are thankful for the financial support through the Ministry of Higher Education under Universiti Teknologi Malaysia for the High-Tech Research Grant with grant number Q.J130000.4623.00Q21.

AUTHOR CONTRIBUTIONS STATEMENT

This journal uses Contributor Roles Taxonomy (CRediT) to recognize individual author contributions, reduce authorship disputes, and facilitate collaboration.

Name of Author	C	M	So	Va	Fo	I	R	D	O	E	Vi	Su	P	Fu
Muhammad Firdaus Ishak	✓	✓	✓	✓	✓	✓	✓	✓	✓	✓	✓		✓	
Mohd Junaidi Abdul Aziz		✓				✓	✓			✓		✓	✓	✓
Mohd Ibthisham Ardani		✓				✓	✓			✓		✓		
Low Wen Yao		✓	✓			✓				✓		✓		
Tole Sutikno						✓	✓			✓		✓		

C : **C**onceptualization
M : **M**ethodology
So : **So**ftware
Va : **Va**lidation
Fo : **Fo**rmal analysis
I : **I**nvestigation
R : **R**esources
D : **D**ata Curation
O : Writing - **O**riginal Draft
E : Writing - Review & **E**diting
Vi : **Vi**sualization
Su : **Su**pervision
P : **P**roject administration
Fu : **Fu**nding acquisition

CONFLICT OF INTEREST STATEMENT

The authors have no competing financial interests or personal relationships that could have appeared to bias the work reported in this paper.

DATA AVAILABILITY

The data that support the findings of this study are available from the corresponding author upon reasonable request.

REFERENCES

[1] K. L. Quade *et al.*, "Benchmarking the transferability of real-time state of charge algorithms to sodium-ion cells using an open-source diagnostics framework," *Batteries & Supercaps*, vol. 9, no. 2, Feb. 2026, doi: 10.1002/batt.202500456.

[2] K. Deshmukh *et al.*, "Sodium-ion batteries: state-of-the-art technologies and future prospects," *Journal of Materials Science*, vol. 60, no. 8, pp. 3609–3633, Feb. 2025, doi: 10.1007/s10853-025-10671-6.

[3] L. Zhao *et al.*, "Engineering of Sodium-ion batteries: opportunities and challenges," *Engineering*, vol. 24, pp. 172–183, May 2023, doi: 10.1016/j.eng.2021.08.032.

[4] M. Rehm, M. Fischer, M. R. Gomez, M. Schütte, D. U. Sauer, and A. Jossen, "Comparing the electrical performance of commercial sodium-ion and lithium-iron-phosphate batteries," *Journal of Power Sources*, vol. 633, Mar. 2025, doi: 10.1016/j.jpowsour.2025.236290.

[5] J. F. Peters, A. Peña Cruz, and M. Weil, "Exploring the economic potential of sodium-ion batteries," *Batteries*, vol. 5, no. 1, Jan. 2019, doi: 10.3390/batteries5010010.

[6] Z. Zhu, D. Qiao, Y. Huang, J. Zhu, Y. Zheng, and Q. Chen, "Comparative study of performance and hybrid battery configuration of sodium-ion and lithium-ion batteries," *Journal of Energy Storage*, vol. 140, Dec. 2025, doi: 10.1016/j.est.2025.118904.

[7] I. Grobler, H. Banderker, and R. Govindsamy, "Evaluating sodium-ion batteries (SiB) and its applications," in *2025 33rd Southern African Universities Power Engineering Conference (SAUPEC)*, IEEE, Jan. 2025, pp. 1–6, doi: 10.1109/SAUPEC65723.2025.10944345.

[8] S. Wang, F. Gao, H. Tian, Y. Zhang, and W. Pan, "Accurate state-of-charge estimation for sodium-ion batteries based on a low-complexity model with hierarchical learning," *Journal of Energy Storage*, vol. 95, Aug. 2024, doi: 10.1016/j.est.2024.112571.

[9] Y. Wang *et al.*, "A comprehensive review of battery modeling and state estimation approaches for advanced battery management systems," *Renewable and Sustainable Energy Reviews*, vol. 131, Oct. 2020, doi: 10.1016/j.rser.2020.110015.

[10] P. Shrivastava, T. K. Soon, M. Y. I. Bin Idris, and S. Mekhilef, "Overview of model-based online state-of-charge estimation using Kalman filter family for lithium-ion batteries," *Renewable and Sustainable Energy Reviews*, vol. 113, p. 109233, Oct. 2019, doi: 10.1016/j.rser.2019.06.040.

[11] H. Xiang, Y. Wang, K. Li, X. Zhang, and Z. Chen, "A comprehensive study on state-of-charge and state-of-health estimation of sodium-ion batteries," *Journal of Energy Storage*, vol. 72, Nov. 2023, doi: 10.1016/j.est.2023.108314.

[12] M. Hossain, M. E. Haque, and M. T. Arif, "Kalman filtering techniques for the online model parameters and state of charge estimation of the Li-ion batteries: A comparative analysis," *Journal of Energy Storage*, vol. 51, Jul. 2022, doi: 10.1016/j.est.2022.104174.

[13] R. Xiong, J. Cao, Q. Yu, H. He, and F. Sun, "Critical review on the battery state of charge estimation methods for electric vehicles," *IEEE Access*, vol. 6, pp. 1832–1843, 2018, doi: 10.1109/ACCESS.2017.2780258.

[14] M. Liu, J. Li, Y. Wang, S. Guo, L. Zhao, and Z. Wang, "Modeling and simulation of sodium-ion batteries based on the combination of electrochemical mechanism and machine learning," *Green Energy and Intelligent Transportation*, vol. 5, no. 1, Feb. 2026, doi: 10.1016/j.geits.2025.100299.

[15] Y.-F. Feng, J.-N. Shen, Z.-F. Ma, and Y.-J. He, "Equivalent circuit modeling of sodium-ion batteries," *Journal of Energy Storage*, vol. 43, Nov. 2021, doi: 10.1016/j.est.2021.103233.

[16] J. Chen, Z. Xu, F. Zou, and X. Cai, "Accurate state of charge estimation of sodium-ion batteries based on temperature and operating condition correction factors," *Ionics*, vol. 31, no. 7, pp. 6907–6918, Jul. 2025, doi: 10.1007/s11581-025-06361-7.

[17] X. Zuo, X. Fu, X. Han, M. Sun, and Y. Fan, "State of charge estimation for sodium-ion batteries based on LSTM network and unscented Kalman filter," *Batteries*, vol. 11, no. 7, Jul. 2025, doi: 10.3390/batteries11070274.

[18] W. Zhou, Y. Zheng, Z. Pan, and Q. Lu, "Review on the battery model and SOC estimation method," *Processes*, vol. 9, no. 9, Sep. 2021, doi: 10.3390/pr9091685.

[19] S. Tamilselvi *et al.*, "A review on battery modelling techniques," *Sustainability*, vol. 13, no. 18, Sep. 2021, doi: 10.3390/su131810042.

[20] A. Mendis, M. E. Haque, M. T. Arif, A. Gargoom, and M. A. Mahmud, "Modeling, parameter, and state of charge estimation of li-ion battery for electric vehicle application," in *2025 IEEE Industry Applications Society Annual Meeting (IAS)*, IEEE, Jun. 2025, pp. 1–8, doi: 10.1109/IAS62731.2025.11061644.

[21] B. Yang *et al.*, "Classification, summarization and perspectives on state-of-charge estimation of lithium-ion batteries used in electric vehicles: A critical comprehensive survey," *Journal of Energy Storage*, vol. 39, Jul. 2021, doi: 10.1016/j.est.2021.102572.

[22] L. Mamouri, T. Pavot, and T. Mesbahi, "Parameter estimation for a generic na-ion battery model using the curve fitting approach," in *2024 IEEE Vehicle Power and Propulsion Conference (VPPC)*, IEEE, Oct. 2024, pp. 1–5, doi: 10.1109/VPPC63154.2024.10755187.

[23] H. Zhang, Z. Zhang, Y. Deng, and J. Yu, "Accurate Prediction of voltage and temperature for a sodium-ion pouch cell using an electro-thermal coupling model," *Batteries*, vol. 11, no. 8, Aug. 2025, doi: 10.3390/batteries11080312.

[24] H. He, H. Qin, X. Sun, and Y. Shui, "Comparison study on the battery SoC estimation with EKF and UKF Algorithms," *Energies*, vol. 6, no. 10, pp. 5088–5100, Sep. 2013, doi: 10.3390/en6105088.

[25] J. Zhu, X. Liu, and T. Chen, "SOC estimation of sodium-ion batteries based on EKF," in *Poster Volume III The 2025 Twenty-First International Conference on Intelligent Computing July 26-29, 2025 Ningbo, China*, The Society of International Computing, 2025, pp. 3524–3541, doi: 10.65286/icic.v21i3.43740.

[26] Y. Liu *et al.*, "Data-driven internal temperature estimation methods for sodium-ion battery using electrochemical impedance spectroscopy," *Journal of Energy Storage*, vol. 87, May 2024, doi: 10.1016/j.est.2024.111426.

BIOGRAPHIES OF AUTHORS



Muhammad Firdaus Ishak received his bachelor's degree in electrical engineering from Universiti Teknikal Malayisa Melaka (UTEM), Malaysia, and his master' degree in electrical power engineering from Universiti Teknologi Malaysia (UTM), Skudai, Malaysia. He is a Ph.D. candidate at Universiti Teknologi Malaysia in Skudai, Malaysia. His research interests include sodium-ion battery management systems, namely equivalent circuit modelling, online parameter identification, and adaptive state-of-charge prediction. His research focuses on battery modelling, nonlinear state estimation, Kalman filtering, and battery energy storage systems. He can be contacted at email: firdau-00@graduate.utm.my.



Mohd Junaidi Abdul Aziz was born in Kuala Terengganu, Malaysia, in 1979. He received his B.S. and M.S. degrees in electrical engineering from the Universiti Teknologi Malaysia (UTM), Malaysia, in 2000 and 2002, respectively, and his Ph.D. in electrical engineering from the University of Nottingham, Nottingham, England, United Kingdom, in 2008. Since 2008, he has been with the Faculty of Electrical Engineering, UTM, where he is presently an associate professor and Head of the Power Electronics and Drive Research Group (PEDG). His current research interests include power electronics and electric vehicles with a special focus on battery management systems. He can be contacted at email: junaidi@utm.my.



Mohd Ibthisham Ardani received his bachelor's degree in mechanical engineering and his Master of Science in mechanical engineering from Universiti Teknologi Malaysia (UTM), Skudai, Johor, in 2009 and 2012, respectively. Later, he pursued his Ph.D. in mechanical engineering and graduated in 2017 from Imperial College London. Currently, he is a senior lecturer in the Faculty of Mechanical Engineering. He has been working in the realm of energy systems and lithium-ion battery/energy storage, particularly on cell-level electrical and thermal tests, with a decade of experience. His work bridges research and practice through collaboration with government, industry, and academia to accelerate safe, efficient, and circular energy-storage solutions. He can be contacted at email: ibthisham@utm.my.



Low Wen Yao earned his bachelor's degree in electrical engineering from Universiti Teknologi Malaysia (UTM) in 2006, his Master of Engineering in Electrical Engineering from UTM in 2010, and his Doctor of Philosophy (Ph.D.) in electrical engineering from UTM in 2013. Currently, he is with Dyson, Singapore, as an Associate Principal Power Electronics Engineer. His professional and research activities cover power electronics, battery modelling, battery management systems, electric vehicles, energy storage systems, and state-of-charge estimation based on equivalent circuit models and Kalman-filter-based methods. He has a solid academic background in electrical engineering and industrial experience in power electronics and battery applications. He can be contacted at email: wenyaolow@gmail.com.



Prof. Ir. Tole Sutikno, S.T., M.T., Ph.D., MIET, IPM., ASEAN Eng. is a lecturer and the head of the master program of electrical engineering at the Faculty of Industrial Technology, Universitas Ahmad Dahlan (UAD) in Yogyakarta, Indonesia. In addition to leading the master program, he also lectures in the Ph.D. Program in informatics and the undergraduate program in electrical engineering at UAD. He received his Bachelor of Engineering from Universitas Diponegoro in 1999, Master of Engineering from Universitas Gadjah Mada in 2004, and Doctor of Philosophy in electrical engineering from Universiti Teknologi Malaysia in 2016. All three degrees are in the electrical engineering area. He has been a professor at UAD in Yogyakarta, Indonesia, since July 2023, following his tenure as an associate professor in June 2008. He is the Editor-in-Chief of TELKOMNIKA and Head of the Embedded Systems and Power Electronics Research Group (ESPERG). He is listed as one of the top 2% of researchers worldwide, according to Stanford University and Elsevier BV's list of the most influential scientists from 2021 to the presents. His research interests cover digital design, industrial applications, industrial electronics, industrial informatics, power electronics, motor drives, renewable energy, FPGA applications, embedded systems, artificial intelligence, intelligent control, digital libraries, and information technology. He can be contacted at email: tole@te.uad.ac.id or thsutikno@ieee.org.